Nanoscale

Symbiotic Assembly of Peptide Nano-Mosaics at Solid Interfaces

Journal:	*Nanoscale*
Manuscript ID	NR-ART-10-2020-007208.R3
Article Type:	Paper
Date Submitted by the Author:	22-Mar-2021
Complete List of Authors:	Jorgenson, Tyler; University of Washington, Molecular Engineering and Sciences Institute Zareie, Hadi; University of Washington, Material Science and Engineering Sarikaya, Mehmet; University of Washington, Materials of Science and Engineering Overney, Rene; University of Washington, Chemical Engineering

ARTICLE

Symbiotic Assembly of Peptide Nano-Mosaics at Solid Interfaces

Tyler D. Jorgenson,[a] Hadi M. Zareie,[b] Mehmet Sarikaya [a, b] and René M. Overney* [a, c]

Received 00th January 20xx,
Accepted 00th January 20xx

DOI: 10.1039/x0xx00000x

The spontaneous co-organization of distinct biomolecules at interfaces enables many of Nature's hierarchical organizations involving both hard and soft materials. Engineering efforts to mimic such hybrid complexes rely on our ability to rationally structure biomolecules at inorganic interfaces. Control over the nanoscale structure of patterned biomolecules remains challenging due to difficulties in controlling the multifarious interactions involved. This work discusses binary peptide assembly as a means to fabricate biomolecular nano-mosaics at graphite surfaces with predictable structures. Distinct peptide-substrate interactions lead to divergent crystallographic growth directions, molecular scale immiscibility, and a symbiotic assembly phenomenon. We present a symbiotic assembly model that accurately predicts the binary assembly structure relying solely on the constituent peptide nucleation kinetics and molar fractions. The ability to tune such biomolecular nano-mosaic structures facilitates the bottom up fabrication of high-density, multifunctional interfaces for nanotechnology.

Introduction

The co-organization of disparate materials into hierarchically assembled constructs is key to developing functional nano- and biotechnologies. For example, multienzyme complexes enable complex chemical pathways that overcome diffusional limitations, while the nanoscale organization of quantum dots significantly tunes their photophysical properties.[1-7] Critical to the engineering of emerging nanobiotechnologies is the rational organization of inorganic and biological materials. To this end a variety of strategies have been developed, such as enzyme fusions, engineered bacteria, and surface immobilization.[8-14]

Functionalization of surfaces with biomolecules is of particular interest for the development of biosensing, bioelectronic and biofuel cell technologies.[9, 15-18] Efficiencies and efficacies of these systems could be enhanced via biomolecular immobilization strategies that dictate the absorbed biomolecular density, orientation and conformational stability.[9, 15] Detrimental effects, were found for simple physisorption such as protein denaturation and loss of activity, which thus, decreased the overall device functionality.[17] To enhance the control over biomolecular immobilization onto surfaces, several strategies have been developed, which rely on biomolecular modifications involving chemical groups that facilitate surface adsorption and linkage.[19-21] Despite these successes, simultaneous control over the geometrical display, spatial distribution, and organized patterning of biomolecules towards full benefit of the surface functionalization remains limited. This level of control over the microscopic topology of the adsorbates is especially critical for the multiplexed patterning of several biomolecules at solid surfaces.[21]

Biomolecular self-assembly has shown to be a powerful approach to tailor interfaces and materials in both naturally occurring and man-made systems.[22-25] Engineered proteins and peptides have been designed to self-assemble at atomically flat two-dimensional solid surfaces with a variety of organized nanostructures.[26-28] Among these biomolecules, solid binding peptides which are genetically selected through directed evolution for substrate specificity have emerged as a prominent strategy for bio-functionalization of inorganic surfaces.[29-31] Solid binding peptides have been used as molecular building blocks to control surface immobilization and the displaying a variety of nano-entities at solid surfaces.[30, 32, 33] Certain solid binding peptide sequences provide the possibility of hierarchical structuring of materials as they form confluent, long-range ordered nanostructures that are commensurate with the underlying solid's crystal lattice. [34, 35] Additionally, external factors such as pH, temperature, and concentration provide engineering controls over the equilibrium self-assembly structure.[36-38]

The wealth of peptide sequence space allows for the facile implementation of a great multitude of substrate and process tailored biomolecular self-assembly systems. While self-assembling peptides have been successfully implemented to display biomolecules at device interfaces, only recently has the fabrication of binary assembled peptide functionalizations been appreciated and attempted.[39, 40] For example, two sequence differing peptides each known to form ordered surface assemblies would enable highly tuned mixed surface structures with designed functionality. Despite these early realizations, for the rational engineering of biomolecular surface

[a] Molecular Engineering and Sciences Institute, University of Washington, Seattle, WA
[b] Department of Material Science and Engineering, University of Washington, Seattle, WA
[c] Department of Chemical Engineering, University of Washington, Seattle, WA
Electronic Supplementary Information (ESI) available: Example AFM analysis, additional experimental data, and all notes referred to in this paper. See DOI: 10.1039/x0xx00000x

functionalizations with independently tailorable phases, a better understanding of miscibility between disparate peptides and their binary assemblies is of critical importance. Specifically, whether the two peptide components co-assemble into a single crystalline order, or self-sort into separate crystalline phases. Additionally, there exists a need for models that accurately predict the binary assembly structure and identify the key parameters controlling the total surface coverage, density, and size of the self-assembled domains

Towards this goal we investigated the assembly structure of two solution-blended combinatorially selected graphite binding peptides (GrBPs), a wild-type version, WT-GrBP5, and its double serine residue N-terminated analogue, SS-GrBP5. The sequence similarity between WT-GrBP5 and SS-GrBP5 and their high propensity to form long range ordered structures at graphite interfaces, makes them prime candidates for investigating two-dimensional binary assembly and local molecular miscibility. Additionally, WT-GrB5 and SS-GrBP5 were chosen due to their relevance to bioelectronic applications. For instance, prior work demonstrated them to be effective graphene surface functionalizations for biosensing devices.[41] While prior works extensively studied the assembly properties of WT-GrBP5, focusing on an observed amorphous-to-ordered transition and the effects of environmental conditions, the studies lacked a rigorous analysis of the peptide domain nucleation itself.[34, 36] Here, we directly analyze WT-GrBP5 and SS-GrBP5 nucleation kinetics in terms of the classical nucleation theory (CNT). Herein, dubbed as symbiotic assembly of binary peptide mixtures, we provide a rigorous understanding of the complex binary biomolecular patterning at atomically flat crystal interfaces. This symbiotic assembly platform represents a highly tunable method for the fabrication of high-density biomolecular nano-mosaics with wide ranging nanobiotechnological applications, e.g., multiplex biosensing for binary biomarkers, multicomponent bioelectronics, and spatially enhanced quantum dot devices.

Results and discussion

WT-GrBP5 was determined as the strongest graphite-binding peptide from a combinatorial selection process.[34] The addition of two serine residues at the N-terminus, yielding SS-GrBP5, increases the hydrophilicity of the peptide while maintaining other chemical and functional properties, i.e., high-binding affinity, binding strength, and long-range ordered assembly.[36] The chemistry and sequence information of WT-GrBP5 and SS-GrBP5 can be found in Table 1.

Table 1

Peptide Name	Sequence	Molecular Weight (Da)	GRAVY
WT-GrBP5	IMVTESSDYSSY	1381.5	-.242
SS-GrBP5	SSIMVTESSDYSSY	1555.6	-.321

The Grand Average of Hydropathicity Score (GRAVY) identifies the relative hydrophilicity. The more negative the number the more hydrophilic the peptide.

Figures 1(a-f) present 2-hour assemblies of 0.5, 0.75 and 1 μM concentrations of WT-GrBP5 and SS-GrBP5 with indistinguishable confluent, high surface coverage films at 1 μM. Approximate film heights of 1.5 nm for WT-GrBP5 and SS-GrBP5 suggest monolayer assemblies. Both WT-GrBP5 and SS-GrBP5 form six-fold symmetric, long range ordering, as evidenced by fast Fourier transforms (FFTs) (insets of Figures 1(c,f)). As shown in Figures 1(a-c) and 1(d-f), respectively, WT-GrBP5 and SS-GrBP5 exhibit an increase in long-range ordered domains with increasing concentration. Growth differences are noticeable at low peptide concentrations, where SS-GrBP5 exhibits fewer aggregates, slimmer structures, and more ordered domains in comparison to WT-GrBP5. The addressed dissimilarity in the nucleation process of the two peptides, the observed amorphous-like clustering at low concentrations and inherent two-dimensionality (2D) of the system, invites a 2D CNT analysis of the two single phase assemblies.

We consider the energetic nucleation free energy Δg_n for the formation of an assembly cluster to be the sum of the free energies of the bulk crystal phase, Δg_b, and the crystal interface, Δg_s.[42, 43] Δg_b is given by the chemical potential difference of the single peptide (monomer) and the peptide crystal assembly, $\Delta\mu$, the area per monomer, A_m, and the radius of the cluster, r, as $\Delta g_b = \left(\pi r^2/A_m\right)\Delta\mu$. Δg_s is determined from the line tension at the crystal-substrate interface, λ, and the size of the cluster, as $\Delta g_s = 2\pi r\lambda$. Thus, at equilibrium, where the cluster size is determined to be $r \equiv r_c = \lambda A_m/\Delta\mu$, the nucleation free energy is $\Delta g_n = \pi A_m \lambda^2/\Delta\mu$. If we consider further that $\Delta\mu$ is given by the activity α of the system, i.e., $\Delta\mu = kT\ln(\alpha)$, which can be related to the activity coefficient γ, the peptide solution concentration C and the equilibrium concentration C_e, as $\alpha = \gamma\left(C/C_e\right)$, the free energy barrier, Δg_n, associated with a 2D circular critical nuclei is given by,

$$\Delta g_n = \frac{\pi A_m \lambda^2}{kT\left(\frac{C}{C_e} - 1\right)} \quad Eqn.\ 1$$

assuming ideality ($\gamma \approx 1$) for low concentration (see Supplemental Information for more details). k is the Boltzmann constant, T is the absolute solution temperature, and, $\left(C/C_e - 1\right)$ represents the supersaturation or activity of the system. With the nuclei free energy Δg_n, we can express for $C > C_e$ the 2D nucleation rate as follows:

$$\frac{dn}{dt} = Ae^{-\frac{\Delta g_n}{kT}} = Ae^{\left(-\frac{\pi A_m \lambda^2}{(kT)^2\left(\frac{C}{C_e}-1\right)}\right)} = Ae^{\left(\frac{-B}{\left(\frac{C}{C_e}-1\right)}\right)} \quad Eqn.\ 2$$

where n is the number of nuclei, A is a complex pre-exponential factor, and B is a dimensionless factor combining the geometric and energetic parameters of the system. As implied by Eqn. 2, the relationship between the nucleation rate and the peptide concentration is non-linear, which as we present next, will fit our data well.

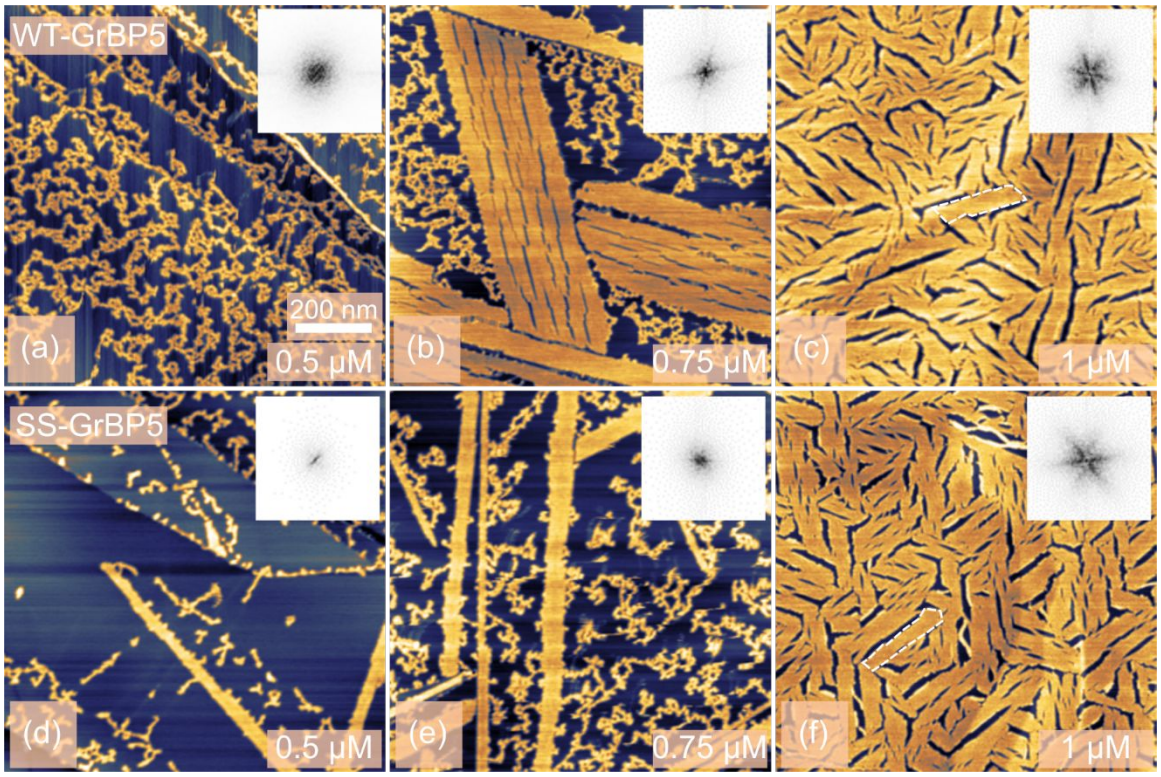

Figure 1. Self-Assembly structures resulting from 2-hour incubations of WT-GrBP5 at (a) 0.5 μM, (b) 0.75 μM, and (c) 1 μM at graphite surfaces. Single component self-assemblies of SS-GrBP5 at the same concentrations (d-f). Scale bar provided in (a) applies to all images.

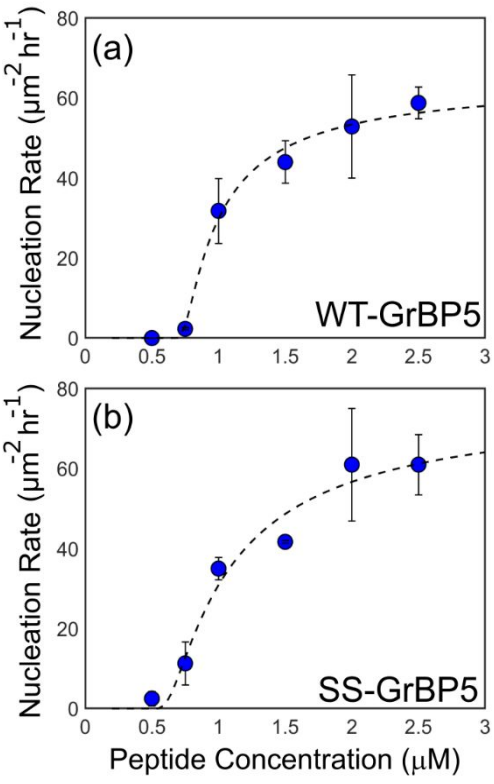

Figure 2. Nucleation rates for (a) WT-GrBP5 and (b) SS-GrBP5. Dotted lines are from Eqn. 2 using fit parameters in Table 2.

Figure 2(a, b) provide the experimentally determined nucleation rate as a function of the peptide concentration, determined from the data in Figure 1 for WT-GrBP5 and SS-GrBP5, respectively. Nucleation rates were estimated from the number of long-range ordered domains per area and incubation time, as described in the experimental section. The nucleation parameters in Table 2 were obtained from the fits in Figure 2. The fit quality let us conclude that WT-GrBP5 and SS-GrBP5 nucleation is well described by the classical 2D nucleation theory. As anticipated from the results in Figure 1, WT-GrBP5 and SS-GrBP5 nucleation kinetics are similar with only subtle differences in fit factors. While the applicability of 2D nucleation theory shown herein is not surprising, we note that the inherent 2D confinement does not preclude the 1D nucleation of peptide nanostructures. As recently investigated by Chen *et al.*, solid binding peptides assembling at MoS_2 interfaces displayed no observable nucleation barrier, and, the nucleation varied linearly with concentration.[35] We attribute the here observed non-linear peptide nucleation processes to the complex relationship between peptide sequence, conformation, intermolecular interactions, and self-assembly. WT-GrBP5 and its mutations self-assembly has previously highlighted this complexity by exhibiting conformational dependent self-assembly that can be (de)activated by thermal pre-processing.[36, 37]

Table 2

Peptide Name	A $(1/\mu m^2 hr)$	B	C_e (μM)
WT-GrBP5	64.9	0.39	0.67
SS-GrBP5	77.1	0.94	0.49

Obtained from fits of Eqn. 2 to the nucleation rates in Fig. 2.

Having obtained an understanding about the individual WT-GrBP5 and SS-GrBP5 self-assembly processes, we focus next on how individual dynamics translates into the binary assembly process involving peptide mixtures. Figure 3 shows the self-assembly structures resulting from 50:50 mixtures of WT-GrBP5 and SS-GrBP5 at total concentrations between 1 and 2 μM. As demonstrated in Figure 3(b) and its inset FFT, the 50:50 mixtures yield high surface coverage monolayers with long-range order. Comparing the microstructures of the mixture (Figure 3) to the single-phase assemblies (Figure 1), it is apparent that the binary self-assembly structure diverges from that of the two pure peptide assemblies. Specifically, comparing the 1 μM total peptide concentration of the binary mixture, Figure 3(a), to the 1 μM single phase systems, Figure 1(c, f), revealed lower surface coverage and less long-range ordering in the binary system. Yet, contrasting the 1 μM 50:50 mixture, Figure 3(a), to the equivalent concentration of the single-phase peptides, (i.e., 0.5 μM WT-GrBP5 and SS-GrBP5) in Figure 1(a, d), reveals a higher degree of ordering in the binary system. Moreover, as highlighted by white dashed outlines in Figures 1(c) and 3(a), the size of the ordered domains in the binary 50:50 mixture is on average ~0.4 times the size of the ordered domains present in pure WT-GrBP5 or SS-GrBP5 assemblies of equal total concentration. Collectively, these results suggest that WT-GrBP5 and SS-GrBP5 are immiscible, and, nucleate and grow their long-range ordered structures competitively.

Nearly right-angle growth patterns form in the 50:50 binary assembly mixtures, Fig. 4(a), which break from the six-fold symmetry found for single phase systems. Thus, it can be concluded that the peptides competitively grow along well-defined substrate induced growth directions. The presence of the close to right-angles documents a ~20° to 30° offset between the WT-GrBP5 and SS-GrBP5 crystallographic assembly directions. Closer FFT analysis of angles in Figure 3 reveal a 24° ± 7° offset between FFT features. Comparing the single-phase self-assembly direction with the 0001 direction of the underlying graphite lattice reveals that WT-GrBP5 assembles at an orientation of 1° ± 7° relative to the zig-zag direction, Figure 4(c), while SS-GrBP5 grows along an angle of approximately 22° ± 6° from the zig-zag direction, Figure 4(d). The difference between the two growth orientations yields an offset of approximately 21° ± 9° between WT-GrBP5 and SS-GrBP5 assemblies, a result within the error of the FFT analysis. The assembly directions of WT-GrBP5 and SS-GrBP5 are schematized in Figure 4(b) depicting the expected offset of ~81°. The divergent growth directions for WT-GrBP5 and SS-GrBP5 provide a molecular rational for the observed immiscibility and competitive assembly. While WT-GrBP5 and SS-GrBP5 compete for the same surface area, the orientational, non-congruent growth directions of the two peptides inhibit a strictly molecular co-assembly process. The result demonstrates a *symbiotic growth partitioning* of surface area, yielding a highly organized and dense assembly pattern that surpasses the single-phase assemblies.

To evaluate the nucleation rate in the peptide mixtures, we return to the 2D CNT analysis and extend it by taking the linear superposition of WT-GrBP5 and SS-GrBP5 nucleation kinetics and considering the molar fraction of each component in the binary assembly, Eqn. 3. We set ζ and 1- ζ to be the molar fraction of WT-GrBP5 and SS-GrBP5, respectively, which yield for the binary nucleation rate:

$$\frac{dn}{dt} = \frac{A_{WT}}{\zeta} e^{\left(\frac{-B_{WT}}{\zeta^2\left(\frac{C}{C_{e,WT}} - \zeta\right)}\right)} + \frac{A_{SS}}{(1-\zeta)} e^{\left(\frac{-B_{SS}}{(1-\zeta)^2\left(\frac{C}{C_{e,SS}} - (1-\zeta)\right)}\right)} \quad Eqn.\ 3$$

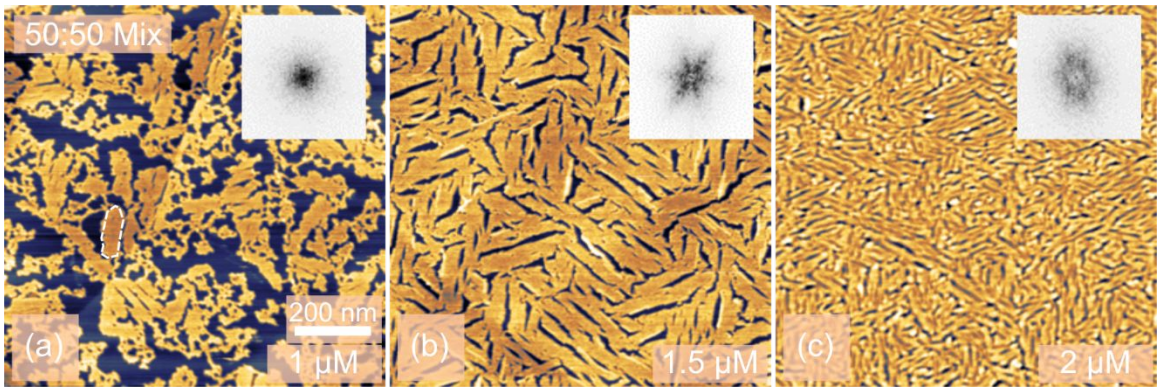

Figure 3. Self-assembly structure resulting from 2-hour incubations of 50:50 mixtures of WT-GrBP5 and SS-GrBP5 with total peptide concentrations of (a) 1 μM, (b) 1.5 μM, and (c) 2 μM. Scale bar in (a) applies to all images.

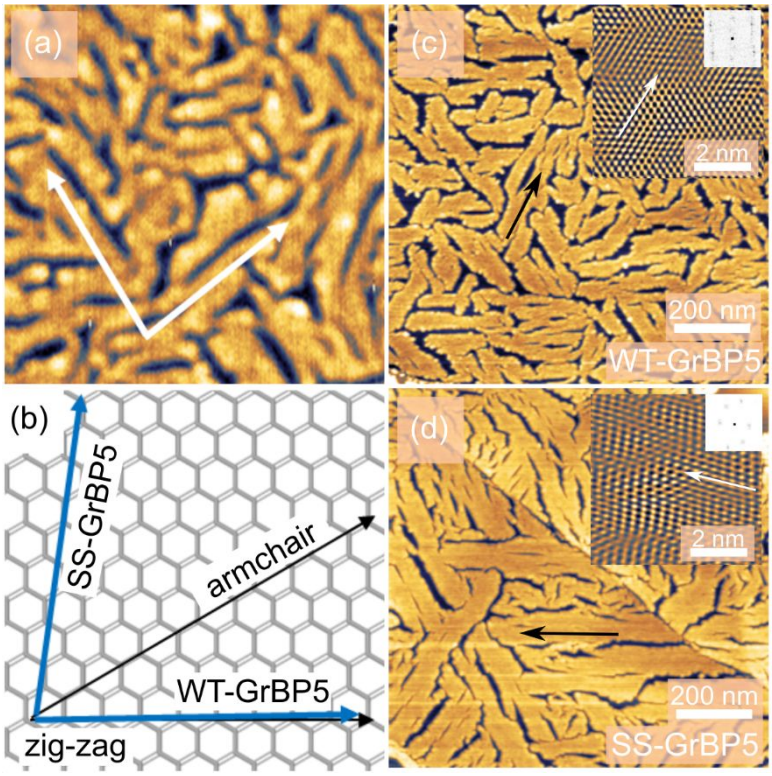

Figure 4. Topology images of (a) 50:50 mixture of WT-GrBP5 and SS-GrBP5 with inset white arrows highlighting the experimentally determined offset. (b) Schematic angle relationship between WT-GrBP5 and SS-GrBP5 with the underlying graphite lattice. The blue arrows indicate major peptide growth directions. (c-d) WT-GrBP5 and SS-GrBP5 assemblies with insets of the FFT filtered underlying graphite atomic lattice. White arrows in (c) and (d) point out the zig-zag direction of the lattice, the black arrows represent the peptide assembly direction.

The introduced molar fraction ζ acts as a scaling parameter to adjust for the concentration dependent competitive growth conditions of the immiscible, binary system. While the molar fraction, ζ, is given by the experimental peptide mixture ratio, the fit parameters A_{WT}, A_{SS}, B_{WT}, B_{SS}, $C_{e,WT}$, and $C_{e,SS}$ were obtained earlier from the single phase assemblies, as provided in Table 2 as A, B, and C_e for WT-GrBP5 and SS-GrBP5, respectively. It is important to note that for Eqn. 3 no new fit parameters were introduced. As shown in Figure 5, an excellent fit is found between Eqn. 3 predicted nucleation rates and the nucleation rates obtained from assembly data shown in Figure 3.

Based on the quality of fit in Figure 5 we find that the introduced scaling of the single-phase nucleation kinetics in Eqn. 3 accurately expresses the observed symbiotic assembly process. The presence of two peptide phases augments the growth partitioning of both phases as evidenced by the increase in the kinetic pre-factors, A_{WT}/ζ and $A_{SS}/(1-\zeta)$. In addition, the two phases cause a divergence from ideality, ($\gamma \neq 1$), i.e., leading to a shift in the supersaturation or increase in the activity, thus, providing a greater driving force for the nucleation process. With the augmentation of the ratios B_{WT}/ζ^2 and $B_{SS}/(1-\zeta)^2$, considering their respective molar fractions, the nucleation rate of the constituent peptides vanishes as expected when its molar fraction approaches zero.

The apparent ad-hoc scaling presented in Eqn. 3 can be justified as follows (for more information see Supplementary Information): We consider that the preexponential factor of the classical nucleation theory for a single phase is given by

$$A = ZjN_s \quad Eqn.\ 4$$

where Z is the Zeldovich factor that accounts for the sticking probability of a molecule onto the critical nuclei, j is the molecular attachment rate, and N_s is the density of nucleation sites.[42] The dynamic quantity Zj can further be approximated using the diffusion coefficient of the nucleus, D, and the mean free path of the monomer, l, as, $Zj = {}^{2D}/_{l^2}$. While D remains unchanged for binary systems, the average area probed by a monomer prior to any collision (assembly attempt), l^2, decreases with decreasing ζ, as the co-existing phase consumes more surface area. This leads to a binary growth partition of $Zj = {}^{2D}/_{\zeta l^2}$ and the kinetic pre-factor A/ζ. Additionally, it must be considered that a decreasing surface area increases the local density of monomers, and thus, reduces C_e with diminishing ζ resulting in a divergence from ideality of $\gamma = 1/\zeta$ and activity $\alpha = \left({}^{C}/_{\zeta C_e}\right)$. The chemical potential difference for the binary system is thus $\Delta\mu = kT[\left({}^{C}/_{C_e}\right) - \zeta]$ for small concentrations. The empirically introduced scaling produces a non-physical limit

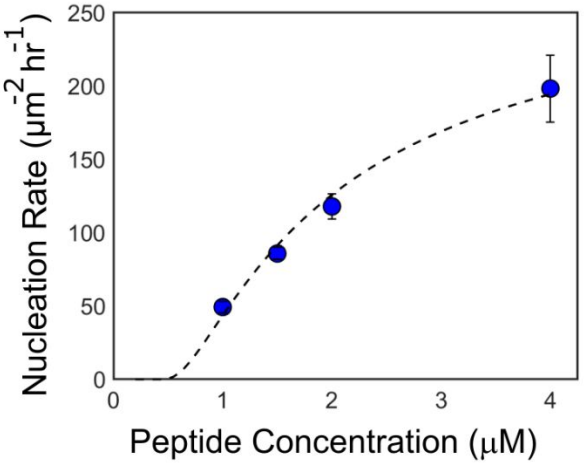

Figure 5. Nucleation rate of 50:50 binary mixture of WT-GrBP5 and SS-GrBP5. Eqn. 3 using fit parameters in Table 2 and ζ of 0.5 results in the dashed black line.

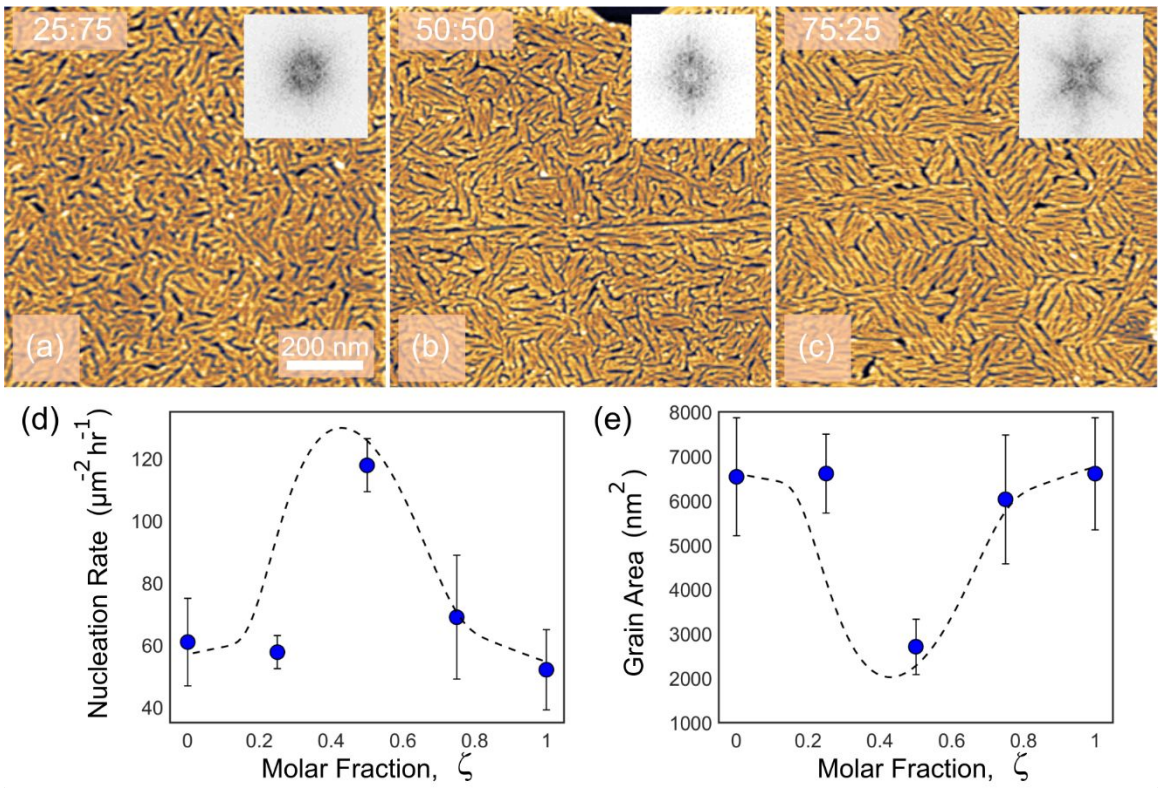

Figure 6. Assembly structure of (a) 25:75, (b) 50:50, and (c) 75:25 mixtures of WT-GrBP5 and SS-GrBP5. Insets are the fast-Fourier transform of the SFM image. (d) nucleation rates and (e) grain area as a function of WT-GrBP5 molar fraction, ζ. Predicted nucleation rate from Eqn. 3 is the black dashed line in (d). The black dashed line in (e) is the predicted grain area using a linear translation of nucleation rates predicted by Eqn. 3. Scale bar in (a) applies to all images.

that for $\zeta \to 0$, $A \to \infty$. To avoid a non-physical limit, Δg_n is augmented to balance the diverging kinetic pre-factor by scaling the line-tension λ/ζ. Thus, for the binary system $B \propto (\lambda/\zeta)^2$. Combined, the outlined implementation of ζ produces the binary nucleation rate as introduced in Eqn. 3 above.

So far, we investigated 50:50 mixtures of WT-GrBP5 and SS-GrBP5. Next, we explore the nucleation rate as a function of the molar fractions for $0 < \zeta < 1$ at a total peptide concentration of 2 μM after an incubation time of two hours. Figure 6(a-c) shows high quality self-assembly structure for 25:75, 50:50, and 75:25 mixtures of WT-GrBP5 and SS-GrBP5. Thus, long-range ordered structures are found to be independent of the molar fraction for a 2 μM total peptide concentration. Figure 6(d) further highlights the validity of our nucleation model (Eqn. 3) by matching the measured nucleation rates. Within the molar fraction range of $0.25 < \zeta < 0.75$ the nucleation rate is augmented significantly over the predominantly single-phase systems with an experimental maximum at $\zeta = 0.5$, by a rate amplification factor of up to two. As documented in Figure 6(e) with the grain area plot *vs.* molar fraction, on average the long-range ordered domains are significantly smaller at $\zeta = 0.5$ compared to the other phase mixtures. At total concentrations above 1 μM, a simple linear relationship exists between the nucleation rate and the grain area allowing the determination of the grain area using Eqn. 3 (see dashed line in Figure 6(e)) Further details are provided in the Supplementary Information. This finding invites single parameter control over the ordered domain size, and thus, bears practical importance for instance for nanoscale patterning of bioreaction cascades to overcome diffusional limitations on reaction rates. Collectively, the results presented in Figure 5 and Figure 6 demonstrate that the molar fraction and total peptide concentration are key parameters controlling the self-assembly structure.

Conclusions

Binary assembly of the two solution-blended combinatorially selected graphite binding peptides, WT-GrBP5 and SS-GrBP5, produced high quality self-assembled monolayers consisting of two immiscible ordered phases. Binary assemblies exhibited equal quality but exceeded in density the single-phase assemblies. The relative orientational difference in the growth-direction of the immiscible phases of approximately 25° could be attributed to the crystallographic growth direction of the single-phase peptides, namely, approximately the zig-zag direction of the graphite lattice for WT-GrBP5 and close to the armchair direction of the graphite lattice for SS-GrBP5. The binary nucleation process was found to function cooperatively, and thus, augmenting the constituent peptide nucleation kinetics in a so-called *"symbiotic"* fashion. Parameters obtained from fitting the single-phase assemblies with a two-dimensional nucleation model, translated seamlessly to describe the symbiotic assembly process using the molar fraction as a scaling parameter. Peptide concentration and peptide molar fraction were found to be the sole critical growth parameters with which the nucleation rate and self-assembly structure can be controlled. The presented binary symbiotic nucleation model is expected to apply to two-dimensional nucleation of binary

systems in which the peptides have similar adsorption kinetics and divergent assembly directions on the substrate. Future work should determine the model's validity for mixtures of peptides with significantly different adsorption and nucleation kinetics.

The summarized results of this symbiotic binary assembly study demonstrate the complexity of peptide miscibility and self-assembly. Since WT-GrBP5 and SS-GrBP5 form separate self-assembled phases, they are immiscible at the molecular scale. However, due to specific peptide-graphite molecular recognition resulting in compatible nucleation and assembly phenomena, WT-GrBP5 and SS-GrBP5 assemblies are apparently miscible at the macroscopic level allowing confluent monolayers. The ability to fabricate polycrystalline interfaces at the macroscopic scale while maintaining molecular level specificity greatly facilitates the development of biomolecular patterned hybrid systems. One could envision controlling the symbiotic assembly of three or more peptides, thus, forming a highly tunable interfacial biomolecular mosaic. To enable the rational design of such bio-inorganic interfaces, further research is needed to understand the role of peptide conformation on peptide-substrate molecular recognition and peptide-peptide intermolecular interactions. As seen with other peptide-substrate systems, computational simulations are well-suited to further explore such molecular phenomena of the bio-inorganic interface.[35, 44-46] The authors hope the summarized experimental results may further guide these key molecular simulations. Additionally, ex-vivo studies of protein/peptide fibrillation at carbonaceous surfaces may be benefitted by the presented results on peptide-surface interactions and self-assembly.[47] Collectively, the presented results demonstrate the ability to control and predict the supramolecular patterning of bio-inorganic interfaces *via* symbiotic assembly of binary peptides, thus enabling the fabrication of multiplexed biomolecular electronics, biofuel cells, and quantum dot technologies.

Experimental

Peptide Synthesis and Assembly

The graphite binding peptides were synthesized on a preloaded support resin using HBTU activation chemistry and Fmoc deprotection as previously described.[36] Synthesized peptides were purified by HPLC (Waters Deltaprep 600, Semiprep Mode) using linear gradients of 1% per minute at a flow rate of 10 mL/min. MALDI-TOF mass spectrometry with reflectron (RETOF-MS, Autoflex II, Bruker Daltonics, Billerica, MA) was used to confirm the purified peptides' molecular weight. The peptide N- and C- termini are left unmodified.

Lyophilized peptides were dissolved in DI water and serially diluted to the experimentally tested ranges. Peptide solutions are kept in hydrophilic Eppendorf tubes to prevent concentration changes over storage time, as GrBP5s have been shown to have lower binding affinity to hydrophilic surfaces. Peptide solutions were limited to 2 freeze thaw cycles to further prevent aging or concentration decreases. All self-assembly samples were prepared on freshly cleaved highly oriented pyrolytic graphite (HOPG grade 1, SPI, Inc.) with an approximate area of 0.25 cm^2. Cleaved graphite surfaces were incubated with 40 µL of peptide in DI water for 2 hours with a variable peptide concentration in an enclosed chamber with saturated water vapor at ambient pressure to prevent evaporation during the assembly process. Peptide solutions were wicked from the incubated graphite surfaces. Residual solution was blown from the graphite surface and dried using a stream of nitrogen. The drying process has been shown to provide reproducible self-assembly structures analogous to in-situ imaged aqueous samples or freeze-dried samples.[34] Several samples were prepared for each peptide concentration and mixture condition. Moreover, samples were prepared using various peptide dilutions to capture variability in concentration between dilutions.

Scanning Force Microscopy (SFM) Imaging

The self-assembly structure of the dried samples was visualized under ambient conditions using a DI Nanoscope IIIa SPM (Digital Instruments) in tapping mode using soft tapping mode SFM probes (HQ:NSC14, MikroMasch). Atomic resolution of the graphite lattice was obtained using a DI Nanoscope IIIa SPM in contact mode with appropriate SFM probes (VistaProbes).

Assembly Structure Analysis

SFM images were analyzed using the Gwyddion SPM data analysis software.[48] Features in the fast Fourier transforms (FFTs) of the SFM images were used to determine the relative angles of the (i) peptide nanostructures in co-assemblies as well as between (ii) peptide nanostructures and the graphite lattice. All analyzed images were 1×1 µm in size. As the broad structure of the peptide nanowires impedes the clear distinction between directions in the FFT, SFM images were first masked to distinguish the peptide nanostructure from the graphite substrate. The mask was then binarized and Fourier analysis was performed on the binarized image. Angles within the FFT were measured by hand. Angles were extracted from three images of each peptide assembly condition from which averages and standard deviations were determined. Samples of WT-GrBP5 and SS-GrBP5 co-assemblies were averaged together. Beyond angles present in the self-assembled peptide nanostructures, the size and density of unidirectional ordered domains, or grains, was analyzed. The density of grains was used to estimate the nucleation rate of the long-range ordered structures. Thereby, we assumed that the number of ordered domains is equivalent to the number of nuclei and that minimal coarsening occurred. Masks separating the peptide from the graphite surface were manually edited to separate these grains. The grain density and average area were averaged over at least three different SFM images and multiple samples.

Author contributions

T.D.J, H.M.Z., M.S., and R.M.O. designed the experiments and did the experimental analysis, T.D.J. and H.M.Z. conducted the experiments. All the authors discussed the results, and T.D.J. and R.M.O wrote the manuscript.

Conflicts of interest

There are no conflicts to declare.

Acknowledgements

This research was primarily supported by NSF DMREF-MGI Grants DMR-1629071, 1848911, and 1922020 which supported T.D.J. and provided all materials and supplies.

References

1. B. S. Winkel, *Annu. Rev. Plant Biol.*, 2004, **55**, 85-107.
2. K.-H. Suss, C. Arkona, R. Manteuffel and K. Adler, *Proceedings of the National Academy of Sciences*, 1993, **90**, 5514-5518.
3. M. Castellana, M. Z. Wilson, Y. Xu, P. Joshi, I. M. Cristea, J. D. Rabinowitz, Z. Gitai and N. S. Wingreen, *Nature biotechnology*, 2014, **32**, 1011-1018.
4. I. Wheeldon, S. D. Minteer, S. Banta, S. C. Barton, P. Atanassov and M. Sigman, *Nature chemistry*, 2016, **8**, 299.
5. J. H. Bang and P. V. Kamat, *ACS nano*, 2009, **3**, 1467-1476.
6. J.-H. Song, T. Atay, S. Shi, H. Urabe and A. V. Nurmikko, *Nano letters*, 2005, **5**, 1557-1561.
7. M. Wang, S. Kumar, A. Lee, N. Felorzabihi, L. Shen, F. Zhao, P. Froimowicz, G. D. Scholes and M. A. Winnik, *Journal of the American Chemical Society*, 2008, **130**, 9481-9491.
8. R. J. Conrado, J. D. Varner and M. P. DeLisa, *Current opinion in biotechnology*, 2008, **19**, 492-499.
9. F. Jia, B. Narasimhan and S. Mallapragada, *Biotechnology and bioengineering*, 2014, **111**, 209-222.
10. J. E. Dueber, G. C. Wu, G. R. Malmirchegini, T. S. Moon, C. J. Petzold, A. V. Ullal, K. L. Prather and J. D. Keasling, *Nature biotechnology*, 2009, **27**, 753.
11. P. Q. Nguyen, N. M. D. Courchesne, A. Duraj-Thatte, P. Praveschotinunt and N. S. Joshi, *Advanced Materials*, 2018, **30**, 1704847.
12. A. Y. Chen, C. Zhong and T. K. Lu, *Journal*, 2015.
13. T. A. Pham, B. C. Choi and Y. T. Jeong, *Nanotechnology*, 2010, **21**, 465603.
14. P. T. Yin, S. Shah, M. Chhowalla and K.-B. Lee, *Chemical reviews*, 2015, **115**, 2483-2531.
15. D. Samanta and A. Sarkar, *Chemical Society Reviews*, 2011, **40**, 2567-2592.
16. A. Zhang and C. M. Lieber, *Chemical reviews*, 2016, **116**, 215-257.
17. U. T. Bornscheuer, *Angewandte Chemie International Edition*, 2003, **42**, 3336-3337.
18. N. Hildebrandt, *Acs Nano*, 2011, **5**, 5286-5290.
19. V. Georgakilas, J. N. Tiwari, K. C. Kemp, J. A. Perman, A. B. Bourlinos, K. S. Kim and R. Zboril, *Chemical reviews*, 2016, **116**, 5464-5519.
20. J. N. Talbert and J. M. Goddard, *Colloids and Surfaces B: Biointerfaces*, 2012, **93**, 8-19.
21. R. Ganesan, K. Kratz and A. Lendlein, *Journal of Materials Chemistry*, 2010, **20**, 7322-7331.
22. N. Stephanopoulos, J. H. Ortony and S. I. Stupp, *Acta materialia*, 2013, **61**, 912-930.
23. S. Zhang, *Nature biotechnology*, 2003, **21**, 1171.
24. N. C. Seeman and H. F. Sleiman, *Nature Reviews Materials*, 2017, **3**, 1-23.
25. J. Fu, Y. R. Yang, A. Johnson-Buck, M. Liu, Y. Liu, N. G. Walter, N. W. Woodbury and H. Yan, *Nature nanotechnology*, 2014, **9**, 531.
26. X. Ma, S. Zhang, F. Jiao, C. J. Newcomb, Y. Zhang, A. Prakash, Z. Liao, M. D. Baer, C. J. Mundy and J. Pfaendtner, *Nature materials*, 2017, **16**, 767-774.
27. H. Pyles, S. Zhang, J. J. De Yoreo and D. Baker, *Nature*, 2019, **571**, 251-256.
28. H. Rapaport, K. Kjaer, T. R. Jensen, L. Leiserowitz and D. A. Tirrell, *Journal of the American Chemical Society*, 2000, **122**, 12523-12529.
29. T. R. Walsh and M. R. Knecht, *Bioconjugate chemistry*, 2019, **30**, 2727-2750.
30. A. Care, P. L. Bergquist and A. Sunna, *Trends in biotechnology*, 2015, **33**, 259-268.
31. M. Sarikaya, C. Tamerler, A. K. Y. Jen, K. Schulten and F. Baneyx, *Nat Mater*, 2003, **2**, 577-585.
32. T. Kacar, M. T. Zin, C. So, B. Wilson, H. Ma, N. Gul-Karaguler, A. K. Y. Jen, M. Sarikaya and C. Tamerler, *Biotechnology and Bioengineering*, 2009, **103**, 696-705.
33. M. Hnilova, D. Khatayevich, A. Carlson, E. E. Oren, C. Gresswell, S. Zheng, F. Ohuchi, M. Sarikaya and C. Tamerler, *Journal of colloid and interface science*, 2012, **365**, 97-102.
34. C. R. So, Y. Hayamizu, H. Yazici, C. Gresswell, D. Khatayevich, C. Tamerler and M. Sarikaya, *ACS Nano*, 2012, **6**, 1648-1656.
35. J. Chen, E. Zhu, J. Liu, S. Zhang, Z. Lin, X. Duan, H. Heinz, Y. Huang and J. J. De Yoreo, *Science*, 2018, **362**, 1135-1139.
36. T. D. Jorgenson, D. T. Yucesoy, M. Sarikaya and R. M. Overney, *Langmuir*, 2019, DOI: 10.1021/acs.langmuir.9b02425.
37. T. D. Jorgenson, M. Milligan, M. Sarikaya and R. M. Overney, *Soft matter*, 2019, **15**, 7360-7368.
38. T. Seki, C. R. So, T. R. Page, D. Starkebaum, Y. Hayamizu and M. Sarikaya, *Langmuir*, 2017, **34**, 1819-1826.
39. P. Li, K. Sakuma, S. Tsuchiya, L. Sun and Y. Hayamizu, *ACS applied materials & interfaces*, 2019, **11**, 20670-20677.
40. L. Sun, T. Narimatsu, S. Tsuchiya, T. Tanaka, P. Li and Y. Hayamizu, *RSC advances*, 2016, **6**, 96889-96897.
41. D. Khatayevich, T. Page, C. Gresswell, Y. Hayamizu, W. Grady and M. Sarikaya, *Small*, 2014, **10**, 1505-1513.
42. R. P. Sear, *Journal of Physics: Condensed Matter*, 2007, **19**, 033101.
43. J. J. De Yoreo and P. G. Vekilov, *Reviews in mineralogy and geochemistry*, 2003, **54**, 57-93.
44. X. Wang, J. K. Weber, L. Liu, M. Dong, R. Zhou and J. Li, *Nanoscale*, 2015, **7**, 15341-15348.
45. Z. He and R. Zhou, *Nanoscale*, 2020.
46. Z. E. Hughes and T. R. Walsh, *Nanoscale*, 2018, **10**, 302-311.
47. C. Li and R. Mezzenga, *Nanoscale*, 2013, **5**, 6207-6218.
48. D. Nečas and P. Klapetek, *Open Physics*, 2012, **10**, 181-188.